Replica symmetry breaking in a diluted network with binary couplings

J. Iwanski, J. Schietse, and M. Bouten
Limburgs Universitair Centrum, B-3590 Diepenbeek, Belgium
(Received 19 December 1994)

We describe a one-stage replica-symmetry-breaking (RSB) calculation of the free energy of the annealed-dilution network with binary couplings. We locate the extremum of the free-energy functional through a systematic search in the space of order parameters. A genuine RSB extremum only exists for values of the storage ratio α greater than α_s, which is the value for which the RS entropy vanishes at $T=0$. The corresponding free energy always has a positive value from which we derive that the storage capacity is equal to α_s. The free energy also determines the fraction of errors when the loading of the network exceeds the storage capacity. Although the error fraction for weak overloading is remarkably small, the information content in the optimal coupling vector fails to grow above its value at saturation.

PACS number(s): 87.10.+e, 64.60.Cn

I. INTRODUCTION

The replica method [1] has evolved over the past ten years into one of the basic tools for the statistical study of neural networks. The method has been highly successful in networks with continuous connection strengths [2–4], where the assumption of replica symmetry (RS) can often be justified. This assumption renders the calculations straightforward and fairly simple. In the case of networks with discrete connection strengths, however, it has turned out to be necessary to proceed to replica symmetry breaking (RSB), which leads to calculations that are considerably more elaborate and laborious.

An important contribution to this development has been Krauth and Mézards' one-stage RSB calculation of the storage capacity for the network with binary couplings [5]. These authors found, for values of the storage ratio α larger than 0.83, that a transition temperature exists below which the system freezes into its ground state with a fraction of the presented patterns not memorized. for values of α smaller than 0.83, however, RS holds good and all patterns are safely stored. Krauth and Mézard additionally found that the critical storage value $\alpha_c=0.83$ could also, yet much more easily, be determined by solving the RS saddle-point equations with the added condition that the RS entropy vanishes at $T=0$. This interesting finding has prompted several authors to add the zero-entropy (ZE) condition also in RS calculations for other networks with discrete couplings, presuming that the equivalence observed by Krauth and Mézard might also hold in these other cases. This has been done by Bouten, Komoda, and Serneels [6] for the annealed-dilution network with binary couplings and by Gutfreund and Stein [7] for multiple-valued couplings. Similar and very extensive calculations have recently been carried out by Bollé and Van Mourik [8] for networks with multistate neurons. It has to be kept in mind, though, that no general argument exists that could justify the RSB-ZE equivalence assumed in the above calculations. In studying a network that interpolates between the Hopfield and the pseudoinverse models, Dotsenko and Tirozzi [9] found that the equivalence does not hold. In her study of the generalized Sherrington-Kirkpatrick spin glass with p-spin interactions, Gardner [10] found that, for all $p>2$, the transition to RSB occurs at a temperature where the entropy is positive. Only in the limit $p\to\infty$, where the model becomes equivalent to the random energy model [11,12], does the transition to RSB coincide with the vanishing of the RS entropy.

In this paper, we describe a one-stage RSB calculation for the annealed-dilution model with binary couplings [6]. The primary aim of this calculation is to investigate the validity of the ZE condition as a criterion for the determination of the storage capacity. A further point of considerable interest is the calculation of the minimum fraction of errors the network makes when the storage level surpasses the saturation limit. This quantity has so far been determined only for networks with continuous connection strengths [13,14].

II. REPLICA CALCULATION

The network we consider is a perceptron with N input and 1 output neurons. Each neuron is a two-state unit described by an Ising variable. The network will function as a memory device for storage of $p=\alpha N$ random patterns or input-output pairs $\{\xi^\mu,\zeta^\mu\}$ $(\mu=1,\ldots,p)$, provided N coupling coefficients J_j can be found such that

$$\zeta^\mu=\mathrm{sgn}\left[\sum_{j=1}^{N} J_j\xi_j^\mu\right] \quad (\mu=1,\ldots,p)\ . \tag{1}$$

The annealed-dilution network with binary couplings is specified by the two constraints [6]

$$J_j=0,\pm1\ , \tag{2}$$

$$\sum_{j=1}^{N} J_j^2=fN\ . \tag{3}$$

The parameter $f\in[0,1]$ determines the degree of dilution. For $f=1$, the model reduces to the fully connected network studied by Krauth and Mézard [5]. The storage

capacity $\alpha_c(f)$ is defined in the thermodynamic limit $N\to\infty$, $p\to\infty$ as the largest value of $\alpha=p/N$ for which coupling coefficients J_j can be found that fulfill all conditions [(1)–(3)].

Following the approach of Gardner-Derrida [15], an energy function is defined on the space of coupling vectors **J** which counts the number of stability conditions (1) that are violated. A general expression can then be written down for the associated free energy $F(T)=-(T/N)\langle \ln Z(T)\rangle$ by making use of the replica method [1].

A. Replica symmetry

To proceed with the actual calculation, one has to make an assumption about the general structure of the order parameter matrix. Using the simplest ansatz of replica symmetry, the free energy is obtained as

$$F_{\rm RS}(T)=-T\operatorname*{extr}_{\{q\hat{q}f\}} G_{\rm RS}(q,\hat{q},\hat{f};\alpha,T,f)\ , \tag{4}$$

where

$$G_{\rm RS}=\tfrac{1}{2}f q\hat{q}-f\hat{f}+\int_{-\infty}^{+\infty}Dz\,\ln[1+e^{\hat{f}-\hat{q}/2}2\cosh(\sqrt{\hat{q}}z)]$$
$$+\alpha\int_{-\infty}^{\infty}Dz\,\ln\left[\int_{-\infty}^{\infty}\frac{d\lambda}{\sqrt{2\pi(1-q)}}\exp\left[-\frac{1}{T}\theta[K-\lambda]-\frac{(\lambda-\sqrt{q}z)^2}{2(1-q)}\right]\right]\ , \tag{5}$$

with the usual shorthand notation Dz for the Gaussian measure. The stability parameter K (in all actual calculations, we will choose $K=0$), the order parameter q, and its conjugate $\hat{q}$ are as in [5,6], while $\hat{f}$ is introduced to express the dilution constraint (3). It is easy to write down the three saddle-point equations for the extremum of $G_{\rm RS}$ and to solve them numerically for different values of the external parameters α, T, and f. The resulting free energy $F_{\rm RS}(T)$ exhibits, for all values of f, a qualitative change in its dependence on T when α grows. For small α, the function $F_{\rm RS}(T)$, starting from zero to $T=0$, decreases monotonically with increasing T. This "normal" behavior, however, is lost beyond a certain value $\alpha_s(f)$. For such $\alpha>\alpha_s(f)$, the free energy $F_{\rm RS}(T)$ still starts from zero at $T=0$ but now rises to a maximum at $T=T_c(\alpha,f)$ before declining at higher values of T. Figure 1 illustrates this change in behavior of $F_{\rm RS}(T)$ for the case $f=0.6$ for which $\alpha_s(f)=1.17$ The deviant behavior when $\alpha>\alpha_s(f)$ entails a negative value for the entropy at temperatures below the critical temperature T_c, a clear signal that the RS result for the free energy cannot be correct. The transition value $\alpha_s(f)$ can be characterized by the property that the RS entropy vanishes at $T=0$.

B. One-stage replica symmetry breaking

Assuming that the RS Ansatz is to blame for the negative entropy, we move on to calculate $\langle \ln Z(T)\rangle$ in the first stage of RSB. This yields

$$F^{(1)}_{\rm RSB}(T)$$
$$=-T\operatorname*{extr}_{\{q_0q_1m\hat{q}_0\hat{q}_1\hat{f}\}} G^{(1)}_{\rm RSB}(q_0,q_1,m,\hat{q}_0,\hat{q}_1,\hat{f};\alpha,T,f)\ , \tag{6}$$

where

$$G^{(1)}_{\rm RSB}=\tfrac{1}{2}f(1-m)q_1\hat{q}_1+\tfrac{1}{2}fmq_0\hat{q}_0-f\hat{f}$$
$$+\frac{1}{m}\int_{-\infty}^{+\infty}Dz_0\ln\int_{-\infty}^{+\infty}Dz_1[1+e^{\hat{f}-\hat{q}_1/2}2\cosh(\sqrt{\hat{q}_0}z_0+\sqrt{\hat{q}_1-\hat{q}_0}z_1)]^m$$
$$+\frac{\alpha}{m}\int_{-\infty}^{+\infty}Dz_0\ln\int_{-\infty}^{+\infty}Dz_1\left[\int_{-\infty}^{+\infty}\frac{d\lambda}{\sqrt{2\pi(1-q_1)}}\exp\left[-\frac{1}{T}\theta[K-\lambda]-\frac{(\lambda-\sqrt{q_0}z_0-\sqrt{q_1-q_0}z_1)^2}{2(1-q_1)}\right]\right]^m\ . \tag{7}$$

The extremum now yields six complicated saddle-point equations, and finding a solution different from the RS solution turns out to be a daunting numerical task. We have concentrated on this problem for quite some time, but, in spite of considerable effort, we have failed to find a new solution that satisfies all saddle-point equations. Since some of these equations become ill-defined when $q_1\to 1$, it is conceivable that the numerical search could miss a solution with q_1 close to 1. However, when we take the asymptotic form of the saddle-point equations for $q_1\to 1$, we discover that these equations are incompatible, so that no solution can exist. This result stands out in contrast to the finding of Krauth-Mézard [5], who wrote that a solution to all equations had been found in a region where $q_1\to 1$ at finite T.

To clear up this contradiction, we have carried out a systematic and controlled search for the overall extremum of $G^{(1)}_{\rm RSB}$. Here we mention only the result and

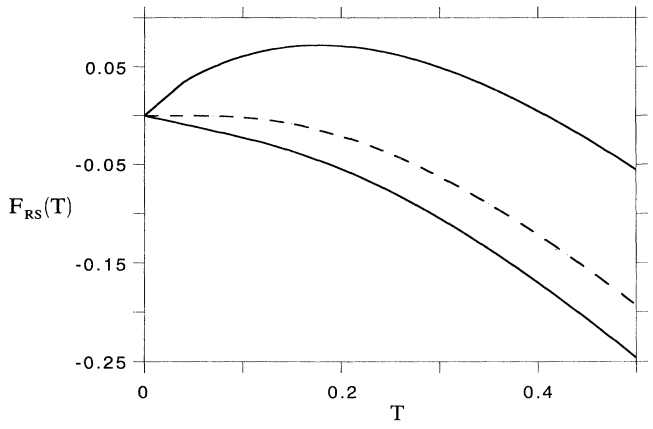

FIG. 1. RS free energy $F_{RS}(T)$ for $f=0.6$ for $\alpha=1.0$ (lower curve), $\alpha=1.17$ (middle curve), and $\alpha=1.4$ (upper curve).

refer to the Appendix for a description of our method. For values of $\alpha>\alpha_s(f)$ and $T<T_c(\alpha,f)$, a genuine RSB extremum, different from the RS solution, exists and it is located in the hyperplane $q_1=1$. This RSB extremum, however, cannot be obtained by searching for solutions of the full set of saddle-point equations because the derivative $\partial G^{(1)}_{RSB}/\partial q_1$ at the extremum is different from zero. For all other values of α and T, the only RSB extremum is the RS solution. Due to the redundancy of the RSB order parameters in this case, the RS solution exists over a large interval of the parameter q_1, extending to the boundary $q_1=1$. We can therefore conclude that the overall extremum of $G^{(1)}_{RSB}$ in the full parameter space can, *in all cases,* be obtained by restricting the search for this extremum to the hyperplane $q_1=1$.

III. THE FREE ENERGY $F^{(1)}_{RSB}(T)$

In order to determine the extremum (6) of $G^{(1)}_{RSB}$ in the hyperplane $q_1=1$, we first derive the asymptotic form of $G^{(1)}_{RSB}$ when $q_1\to 1$. Since $q_1=1$ is at the border of the domain of q_1, its conjugate variable $\hat{q}_1$ must tend to infinity. It is now important to notice that, as $\hat{q}_1\to\infty$, there must be a concurrent growth of $\hat{f}$ in order to keep the dilution degree intermediate between 0 and 1. More explicitly, the combination

$$\hat{r}:=m\hat{f}-\frac{m(1-m)}{2}\hat{q}_1 \tag{8}$$

has to retain a finite value. Once this is noted, it becomes straightforward to calculate the limit of $G^{(1)}_{RSB}$:

$$G^{(1)}_{RSB}\underset{\substack{q_1\to 1\\ \hat{q}_1\to\infty}}{\to}\frac{1}{m}\left\{\tfrac{1}{2}fm^2\hat{q}_0q_0-f\hat{r}+\int_{-\infty}^{+\infty}Dz_0\ln[1+e^{\hat{r}-m^2\hat{q}_0/2}2\cosh(m\sqrt{\hat{q}_0}z_0)]\right\}$$
$$+\alpha\int_{-\infty}^{+\infty}Dz_0\ln\left[\int_{-\infty}^{+\infty}\frac{d\lambda}{\sqrt{2\pi(1-q_0)}}\exp\left[-\frac{m}{T}\theta[K-\lambda]-\frac{(\lambda-\sqrt{q_0}z)^2}{2(1-q_0)}\right]\right]. \tag{9}$$

Comparison with (5) shows that this asymptotic form is related to G_{RS} in a simple way,

$$G^{(1)}_{RSB}\underset{\substack{q_1\to 1\\ \hat{q}_1\to\infty}}{\to}\frac{1}{m}G_{RS}\left[q_0,m^2\hat{q}_0,\hat{r};\alpha,\frac{T}{m},f\right]. \tag{10}$$

Using this simplified expression for $G^{(1)}_{RSB}$ in (6) we obtain

$$F^{(1)}_{RSB}(T)=\underset{\{q_0m\hat{q}_0\hat{r}\}}{\text{extr}}\left[-\frac{T}{m}G_{RS}\left[q_0,m^2\hat{q}_0,\hat{r};\alpha,\frac{T}{m},f\right]\right]. \tag{11}$$

The main difference with the expression (4) for $F_{RS}(T)$ is the occurrence of the extra variable m in the extremum operation. However, if we rewrite (11) as

$$F^{(1)}_{RSB}(T)=\underset{m}{\text{extr}}\left\{\underset{\{q_0\hat{q}_0\hat{r}\}}{\text{extr}}\left[-\frac{T}{m}\times G_{RS}\left[q_0,m^2\hat{q}_0,\hat{r};\alpha,\frac{T}{m},f\right]\right]\right\}, \tag{12}$$

comparison with (4) immediately shows that

$$F^{(1)}_{RSB}(T)=\underset{m}{\text{extr}}F_{RS}\left[\frac{T}{m}\right]. \tag{13}$$

The extremum in this expression is a maximum and the value of m must be confined to the interval [0,1]. Calling $T'=T/m$, we can rewrite (13) in the more appealing form

$$F^{(1)}_{RSB}(T)=\max_{T'\geq T}F_{RS}(T'). \tag{14}$$

Our previous study of $F_{RS}(T)$ in Fig. 1 allows us now to determine $F^{(1)}_{RSB}(T)$ immediately for any value of α. For $\alpha<\alpha_s(f)$, $F_{RS}(T)$ is a monotonically decreasing function so that the maximum in (14) is obtained at the lower bound $T'=T$. The same argument applies for $\alpha>\alpha_s(f)$ when $T>T_c(\alpha,f)$. In the remaining case, $\alpha>\alpha_s(f)$ and $T>T_c(\alpha,f)$, the maximum is obtained at $T'=T_c(\alpha,f)$. Thus we finally obtain

$$F^{(1)}_{RSB}(T)=\begin{cases}F_{RS}[T_c(\alpha,f)] & \text{if } \alpha>\alpha_s(f) \text{ and } T<T_c(\alpha f)\\ F_{RS}(T) & \text{otherwise}.\end{cases} \tag{15}$$

IV. RESULTS AND DISCUSSION

It is now easy to determine the storage capacity of the annealed-dilution network. This is characterized as the storage level where the network loses its ability of storing all input-output relations perfectly. This translates to the energy function starting to take on a nonzero value. The ground-state energy as a function of α follows from (15):

$$E_0(\alpha,f)=\begin{cases} F_{\rm RS}(T_c(\alpha,f)) , & \alpha>\alpha_s(f) \\ F_{\rm RS}(0), & \alpha<\alpha_s(f) . \end{cases} \tag{16}$$

From our previous study of $F_{\rm RS}(T)$, we know $F_{\rm RS}(0)=0$ and $F_{\rm RS}(T_c(\alpha_c,f))>0$. Hence we immediately conclude

$$\alpha_c(f)=\alpha_s(f) . \tag{17}$$

This vindicates the ZE assumption made in [6] to determine the storage capacity $\alpha_c(f)$ of the annealed-dilution network with binary couplings. Figure 2 shows the storage capacity $\alpha_c(f)$ and compares the theoretical curve with results from numerical simulations for $N=12$ and 16 neurons. These results were obtained through a full enumeration of all coupling vectors **J** that satisfy the constraints (2) and (3). Like Krauth and Opper [16], we have chosen "Gaussian" random patterns in order to avoid the strong odd-even effects that occur in systems of a small size. Choosing a set of $p=\alpha N$ random input vectors and a random binary output, we scan all possible coupling vectors **J** to find out whether or not a vector exists that stores all the patterns. Repeating this process for many samples determines the probability of success, which then determines the storage capacity. The figure shows remarkably good overall agreement between the theoretical curve and the simulations. Nevertheless, one should be very cautious in drawing conclusions from this agreement, as it is well known that strong finite-size effects [17] may invalidate the good agreement observed in simulations with small N. A comparison of our results for $N=12$ and $N=16$ gives us some hint of the importance of finite-size effects. Since, for given N, the value of f increases in jumps of $1/N$, a good comparison is only possible for such values of f that are multiples of $\frac{1}{12}$ and $\frac{1}{16}$, i.e., the multiples of $\frac{1}{4}$. At these points, we find that the results for $N=16$ move slightly closer to the theoretical curve than those for $N=12$. This gives us some confidence that the theoretical curve may represent the correct storage capacity. Simulations for considerably larger values of N would be needed to confirm or invalidate this confidence, but they are not feasible for a full enumeration procedure.

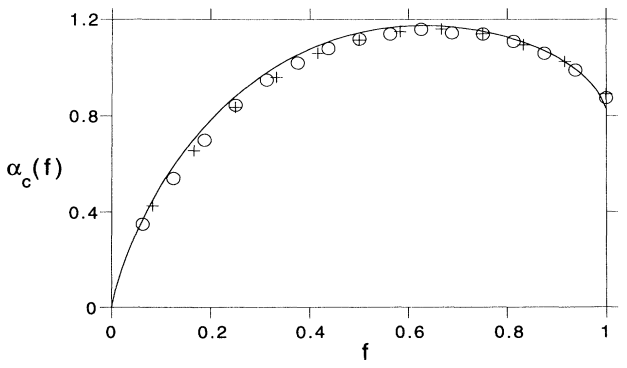

FIG. 2. Storage capacity $\alpha_c(f)$ as a function of the fraction of nonzero couplings. The theoretical curve is compared to numerical results, obtained from a full enumeration of coupling vectors for a network with $N=12$ (+) and $N=16$ (○) neurons.

Besides the storage capacity, knowledge of $E_0(\alpha,f)$ also allows us to determine the minimal fraction of errors in the output when the loading exceeds the storage capacity. For $\alpha>\alpha_c(f)$, the fraction of errors is given by

$$e(\alpha,f)=\frac{1}{p}E_0(\alpha,f)=\frac{1}{\alpha N}F_{\rm RS}(T_c(\alpha,f)) . \tag{18}$$

Results from our numerical calculations of $E_0(\alpha,f)$ are shown in Fig. 3(a) for three choices of the dilution parameter $f=0.3$, 0.6, and 1. The three curves display a very similar behavior, starting from 0 at $\alpha_c(f)$ and rising slowly towards the asymptotic value 0.5 when $\alpha\to\infty$. The great similarity of the curves becomes even more apparent when we rescale the α axis and plot $e(\alpha,f)$ as a function of the "relative degree of overloading" $\alpha/\alpha_c(f)$ [Fig. 3(b)]. The two curves for $f=0.3$ and 1 now become indistinguishable on the scale of the figure, while the $f=0.6$ curve comes slightly below, the deviation always being smaller than 3%. For the sake of simplicity, we will in the following discussion ignore these small deviations and consider $e(\alpha,f)$ as a function of $\alpha/\alpha_c(f)$.

To appreciate the performance of the minimization of errors procedure, it is useful to compare the calculated value of $e(\alpha,f)$ to some standard. A reasonable choice is the following coupling vector. Among the $p=\alpha N$ patterns, we take at random any subset of $\alpha_c(f)N$ patterns and determine the coupling vector (denoted by $\mathbf{J}^*$) that stores this subset exactly. Of the remaining $[\alpha-\alpha_c(f)]N$ patterns, half will on average be classified correctly by $\mathbf{J}^*$, while the other half will get the wrong output. The fraction of errors for the network with coupling vector $\mathbf{J}^*$ is then

$$e^*(\alpha,f)=\frac{1}{2}\left[1-\frac{\alpha_c(f)}{\alpha}\right] , \quad \alpha\geq\alpha_c(f) . \tag{19}$$

This function is also shown in Fig. 3(b) (dotted line). It obviously is an upperbound for the minimal fraction of errors $e(\alpha,f)$. A comparison of the curves indicates that $e(\alpha,f)$ lies well below $e^*(\alpha,f)$ for not too large values of α/α_c. As an example, for $\alpha/\alpha_c=2$, the minimal fraction of errors is $e=0.11$, to be compared to $e^*=0.25$. This means that, when the network is overloaded with as many extra patterns as it can properly store at saturation, it is possible to reduce the 50% wrong outputs on the extra patterns made by the vector $\mathbf{J}^*$ to a mere 22% by selecting the optimal coupling vector. In the case of continuous couplings [13,14], the minimal fraction of errors is even lower (as can be read off from the published figures). Minimizing the fraction of errors thus appears to be an efficient way to improve the storage performance

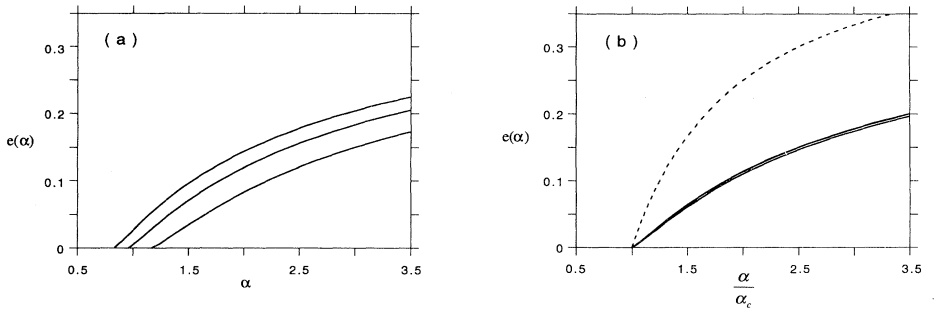

FIG. 3. (a) Fraction of errors $e(\alpha,f)$ as a function of α for $f=0.6$ (lower curve), $f=0.3$ (middle curve), and $f=1$ (upper curve). (b) The same curves as α function of $\alpha/\alpha_c(f)$ for $f=0.6$ (lower solid curve) and for $f=0.3$ or $f=1$ (upper solid curve). The dotted curve represents the upperbound $e^*(\alpha/\alpha_c)$.

of an overloaded network.

As is well known [6], at the saturation limit $\alpha_c(f)$ the amount of information stored in the coupling vector regarding the classification of the $\alpha_c(f)N$ input patterns is markedly below the maximum amount that is possible to store in a vector that satisfies the constraints (2) and (3). The fraction of information storage that still remains available at saturation varies with the dilution f, its largest value exceeding 25% for $f=\frac{2}{3}$. When the network gets overloaded and the optimal coupling vector is found by minimizing the number of wrong outputs, one may expect that some additional information is collected in the optimal vector and that the total information content will continue to grow towards the maximum possible. At loading level $\alpha>\alpha_c(f)$, the information contained in the optimal vector is given by

$$I(\alpha,f)=\alpha N\left[1+\frac{e(\alpha,f)\ln[e(\alpha,f)]+[1-e(\alpha,f)]\ln[1-e(\alpha,f)]}{\ln 2}\right], \tag{20}$$

where $e(\alpha,f)$ is the minimal fraction of errors (18) and $I(\alpha,f)$ is measured in bits. In particular, for $\alpha=\alpha_c(f)$ i.e., at saturation, (20) yields $I(\alpha_c(f),f)=\alpha_c(f)N$. The same value clearly is also the information content of the vector $\mathbf{J}^*$ with the fraction of errors (19). It is important to note that the expression (20) is not applicable for the vector $\mathbf{J}^*$ because in this case, the identity of $\alpha_c(f)N$ patterns that are correctly classified is known. As we have found to a very good approximation that $e(\alpha,f)$ is a function of $\alpha/\alpha_c(f)$, it is expedient to rewrite (20) in the form

$$\frac{I(\alpha,f)}{I(\alpha_c(f),f)}=\frac{\alpha}{\alpha_c}\left[1+\frac{e\left[\frac{\alpha}{\alpha_c}\right]\ln\left[e\left[\frac{\alpha}{\alpha_c}\right]\right]+\left[1-e\left[\frac{\alpha}{\alpha_c}\right]\right]\ln\left[1-e\left[\frac{\alpha}{\alpha_c}\right]\right]}{\ln 2}\right]. \tag{21}$$

This shows that the relative change in the amount of stored information depends only on the relative degree of overloading α/α_c. To a very good approximation, $I(\alpha)/I(\alpha_c)$ will therefore be the same for all values of the dilution f. Numerical evaluation of (21) for different values of f yields the surprising result that $I(\alpha)/I(\alpha_c)$ stays almost constant with a value very close to 1 over an extended interval of $\alpha/\alpha_c\geq 1$. This result is shown in Fig. 4 for $f=0.6$. The linear rise for $\alpha/\alpha_c<1$ is followed by a tiny bump of height less than 1.004 at $\alpha/\alpha_c\sim 1.2$. For larger values of α/α_c the function slopes down very slowly to its asymptotic value 0.995. A very similar behavior has been obtained for other values of f, with the maximum height never exceeding 1.008 and the asymptotic value always larger than 0.96. Contrary to expectation, the information content in the optimal coupling vector never increases substantially above its value at saturation, which is also the information stored in $\mathbf{J}^*$. Even though the number of correctly stored patterns does increase markedly, the corresponding gain of information is compensated almost exactly by the loss of information

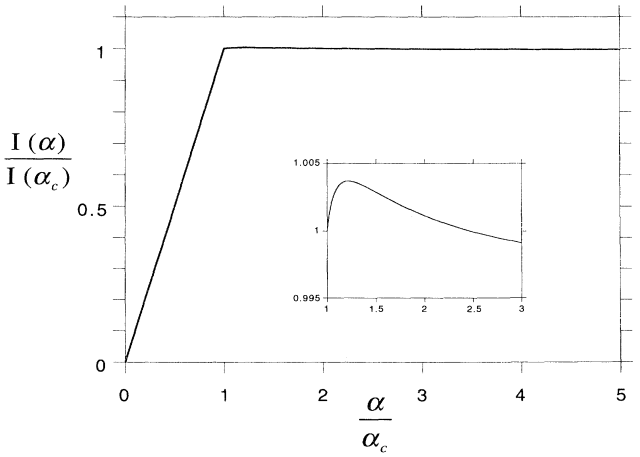

FIG. 4. Information stored in the optimal coupling vector as a function of α/α_c for $f=0.6$. The inset gives a magnified view of the tiny bump at $\alpha/\alpha_c=1.2$.

due to the fact that one does no longer know the identity of αN correctly classified patterns. This result resembles the finding for biased patterns [2], where the substantial increase in the number of stored patterns does not entail an increase in the amount of stored information. One could still hope that an increase in stored information might be achieved by using a more suitable cost function that maximizes the information storage. Nevertheless, since the stored information per pattern is a function only of $e(\alpha,f)$ [see (20)], minimizing the fraction of errors is tantamount to maximizing the information storage. [This conclusion has to be qualified to a certain degree because the expression (20) for $I(\alpha,f)$ is only valid for cost functions that treat the αN patterns in a symmetrical way, which is the type of cost function that has commonly been considered up to now.] The prospects for increasing the information storage in the coupling vector above its value at saturation therefore look rather bleak. Surprisingly, a way has recently been discovered to make full use of all the available information storage of a binary vector by replacing the signum operation in (1) by a more complicated activation function [18].

ACKNOWLEDGMENTS

It is a pleasure to thank Chris Van den Broeck, Andreas Engel, Tamas Geszti, and Michael Wong for useful suggestions and interesting discussions. Financial support has been obtained from the IIKW, Brussels, and from the IUAP Program of the Belgian Government.

APPENDIX

To pin down the location of the overall extremum of $G^{(1)}_{\rm RSB}$ in the six-dimensional parameter space, we will proceed in two steps. In the first step, we determine the extremum of $G^{(1)}_{\rm RSB}$ within each hyperplane with a fixed value for the parameter q_1. This can be done by finding the solution to the saddle-point equations for the five remaining parameters. The value of the extremum obtained in the hyperplane q_1 is denoted as

$$\tilde{G}(q_1)=\underset{\{q_0 m \hat{q}_0 \hat{q}_1 \hat{f}\}}{\rm extr} G^{(1)}_{\rm RSB}(q_0,q_1,m,\hat{q}_0,\hat{q}_1,\hat{f};\alpha,T,f)\ . \tag{A1}$$

In the second step, we make a plot of $\tilde{G}(q_1)$ in the interval [0,1] and locate the extremum (i.e., minimum) value.

We have carried out the above procedure for many different values of the three external parameters, α, f, and T. In all cases considered, it turns out that finding the numerical solution of the five remaining saddle-point equations for any fixed value of q_1 is a straightforward task. Plotting the corresponding value of $\tilde{G}(q_1)$ exhibits two different types of curves, depending on the values of α and T. For small α or large T, the function $\tilde{G}(q_1)$ decreases smoothly with increasing q_1 to a minimum beyond which it stays constant at this minimum value. An example of such curves is shown in Fig. 5(a). For larger α and low T, however, while $\tilde{G}(q_1)$ starts off in the same way and shows a similar behavior over a large part of the q_1 interval, the behavior close to the border $q_1=1$ becomes very different. Here $\tilde{G}(q_1)$ begins to slope down again and, very near $q_1=1$, drops down steeply to its minimum value. Figure 5(b) shows an example where both types of curves are present for different values of T. The value of $\tilde{G}(q_1)$ very close to $q_1=1$ cannot be calculated numerically because the convergence of the integrals in the saddle-point equations deteriorates badly as $q_1\to 1$. But here we can make use of the asymptotic form of the equations, as has been done in Sec. III.

We now turn to Figs. 5(a) and 5(b) for a more detailed discussion of our results. Both figures show $T\tilde{G}(q_1)$ in the interval $0.4\le q_1\le 1$ for the same dilution $f=0.6$ and two different values of the temperature, $T=0.05$ and 0.14. Figure 5(a), for $\alpha=1$, is typical of small α behavior, while Fig. 5(b) for $\alpha=1.4$ is typical of large α behavior. In the figures, we have added the extra factor T to $\tilde{G}(q_1)$ so that the lowermost value of each curve directly indicates the value of the free energy [except for a change in sign; see (6)], which after all is the quantity we are interested in. In Fig. 5(a) for $\alpha=1.0$, the same type of behavior of $\tilde{G}(q_1)$ is observed for *all* values of T (illustrated here for two values only). At low values of q_1, the extremum (A1) yields $q_0=q_1$. The value of $\tilde{G}(q_1)$ decreases rapidly with increasing q_1 until the minimum is reached at $q_{\rm min}=0.62$ for $T=0.05$ and at $q_{\rm min}=0.56$ for $T=0.14$. These minima (indicated by an arrow) represent the RS solution at these two temperatures. The curves can be continued with the RS ansatz for larger values of q_1 (dashed curves) by imposing the extra constraint $q_0=q_1$ in (A1). In our search for the extremum of $G^{(1)}_{\rm RSB}$ however, we must allow q_0 full freedom to take on its optimal value. We then find that $\tilde{G}(q_1)$ stays constant

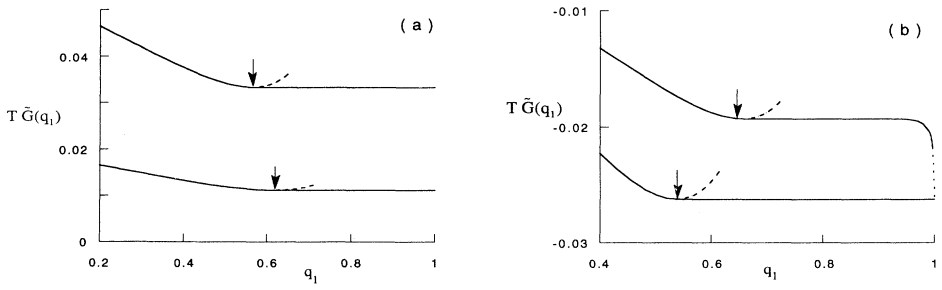

FIG. 5. (a) Function $T\tilde{G}(q_1)$ for $f=0.6$, $\alpha=1.0$ for $T=0.05$ (lower curve), and $T=0.14$ (upper curve). (b) The function $T\tilde{G}(q_1)$ for $f=0.6$, $\alpha=1.4$ for $T=0.14$ (lower curve), and $T=0.05$ (upper curve).

over the whole remaining interval (solid curves). The constancy of $\tilde{G}(q_1)$ is easily understood by noting, for $q_1 > q_{\min}$, that the extremum (A1) systematically yields $m=1$ and $q_0=q_{\min}$. This clearly keeps the Parisi order parameter function unaltered [19]. From Fig. 5(a) one notices that the minimum value of $T\tilde{G}(q_1)$ is positive and decreases with decreasing T. This reflects the behavior of the RS free energy in Fig. 1 in the case $\alpha < \alpha_s(f)$ [recall $\alpha_s(f)=1.17$ for $f=0.6$].

In Fig. 5(b), for $\alpha=1.4$, which is now larger than $\alpha_s(f)$, we observe a different behavior according to whether $T > T_c(\alpha,f)$ or $T < T_c(\alpha,f)$. For all $T \geq 0.14$, which is the value of $T_c(1.4,0.6)$, we observe the same behavior as in Fig. 5(a), with the RS solution a minimum value for $T\tilde{G}(q_1)$. Note that the value at the minimum has become negative now in accordance with the positive RS free energy in this case in Fig. 1. Going to the lower temperature $T=0.05$ raises the RS minimum. More exciting, however, is the different behavior for large values of q_1. Near $q_1=1$, the constant plateau value of $\tilde{G}(q_1)$ begins to slope down again and, very close to the border $q_1=1$, it plunges towards its minimum value at $q_1=1$. We have calculated $\tilde{G}(q_1)$ numerically up to $q_1=0.998$ (solid curve). The dotted line is an extrapolation to the minimum value of $T\tilde{G}(q_1)$ at $q_1=1$, as is obtained in Sec. III. The figure clearly demonstrates that the minimum of $\tilde{G}(q_1)$ is located at $q_1=1$. The slope at the minimum is large and negative, which demonstrates that this minimum cannot be obtained from solving the saddle-point equations.

[1] M. Mézard, G. Parisi, and M. Virasoro, *Spin Glass Theory and Beyond* (World Scientific, Singapore, 1987).
[2] E. Gardner, J. Phys. A **21**, 257 (1988).
[3] K. Y. M. Wong and D. Sherrington, J. Phys. A **23**, 4659 (1990).
[4] M. Griniasti and H. Gutfreund, J. Phys. A **24**, 715 (1991).
[5] W. Krauth and M. Mézard, J. Phys. **50**, 3057 (1989).
[6] M. Bouten, A. Komoda, and R. Serneels, J. Phys. A **23**, 2605 (1990).
[7] H. Gutfreund and Y. Stein, J. Phys. A **23**, 2613 (1990).
[8] D. Bollé and J. Van Mourik, J. Phys. A **27**, 1151 (1994).
[9] V. Dotsenko and B. Tirozzi, J. Phys. A **24**, 516 (1991).
[10] E. Gardner, Nucl. Phys. B **257**, 747 (1985).
[11] B. Derrida, Phys. Rev. B **24**, 2613 (1981).
[12] D. J. Gross and M. Mézard, Nucl. Phys. B **240**, 431 (1984).
[13] R. Erichsen and W. K. Theumann, J. Phys. A **26**, L61 (1993).
[14] P. Majer, A. Engel, and A. Zippelius, J. Phys. A **26**, 7405 (1993).
[15] E. Gardner and B. Derrida, J. Phys. A **21**, 271 (1988).
[16] W. Krauth and M. Opper, J. Phys. A **22**, L519 (1989).
[17] B. Derrida, R. B. Griffiths, and A. Prügel-Bennett, J. Phys. A **24**, 4907 (1991).
[18] G. J. Bex, R. Serneels, and C. Van den Broeck, Phys. Rev. E **51**, 6309 (1995).
[19] G. Parisi, J. Phys. A **13**, 1101 (1980).